PNAS RESEARCH ARTICLE | BIOPHYSICS AND COMPUTATIONAL BIOLOGY

Active emulsions in living cell membranes driven by contractile stresses and transbilayer coupling

Suvrajit Saha[a,b,1], Amit Das[a,c,1], Chandrima Patra[a], Anupama Ambika Anilkumar[a,2], Parijat Sil[a,3], Satyajit Mayor[a,4], and Madan Rao[a,4]

Contributed by Satyajit Mayor; received December 22, 2021; accepted June 6, 2022; reviewed by Patricia Bassereau and Jean Francois Joanny

The spatiotemporal organization of proteins and lipids on the cell surface has direct functional consequences for signaling, sorting, and endocytosis. Earlier studies have shown that multiple types of membrane proteins, including transmembrane proteins that have cytoplasmic actin binding capacity and lipid-tethered glycosylphosphatidylinositol-anchored proteins (GPI-APs), form nanoscale clusters driven by active contractile flows generated by the actin cortex. To gain insight into the role of lipids in organizing membrane domains in living cells, we study the molecular interactions that promote the actively generated nanoclusters of GPI-APs and transmembrane proteins. This motivates a theoretical description, wherein a combination of active contractile stresses and transbilayer coupling drives the creation of active emulsions, mesoscale liquid order (lo) domains of the GPI-APs and lipids, at temperatures greater than equilibrium lipid phase segregation. To test these ideas, we use spatial imaging of molecular clustering combined with local membrane order, and we demonstrate that mesoscopic domains enriched in nanoclusters of GPI-APs are maintained by cortical actin activity and transbilayer interactions and exhibit significant lipid order, consistent with predictions of the active composite model.

nanoscale | mesoscale | plasma membrane | membrane ordering | active mechanics

Significance

Attempts to understand the lateral mesoscale organization of molecules on the cell surface have relied on equilibrium thermodynamic principles. Here, we identify cortical actomyosin as a molecular organizer of local plasma membrane composition. We show using theory and experiments that the mesoscale organization of a large class of membrane proteins and lipids is driven by active contractile stresses and transbilayer lipid-mediated coupling as well as lateral interactions. This generates active emulsions with distinct characteristics and highlights the role of nonequilibrium regulation of lateral membrane organization of both lipids and proteins.

An outstanding issue in modern cell biology is the spatiotemporal organization of composition. The plasma membrane of a living cell with its diversity of proteins and lipids is an archetypal example (1). Numerous studies have revealed that molecular organization at the cell surface, ranging from 10 to 10^3 nm in space and 10^{-3} to 10 s in time, has direct functional consequences for signaling reactions, molecular sorting, and endocytosis (2, 3). Following the fluid-mosaic model (4), several equilibrium models, such as the lipid–shell model (5) and the lipid–raft model (6), have been proposed to describe the lateral organization of the cell membrane. More recently, it has been shown that many cell surface proteins and lipids form dynamic nanoclusters driven by the activity of actomyosin at the cell cortex (7–12). This not only identifies a novel molecular organizer of local plasma membrane composition, namely cortical actomyosin (13–15), but also, a new mechanism, highlighting the role of nonequilibrium, energy-consuming "active" processes (16) in driving local compositional heterogeneities (17).

This is the motivation for the active composite cell surface model (8, 17–19), a juxtaposition of the membrane bilayer and the actomyosin cortex where membrane components that couple to the cortical elements are subject to fluctuating actomyosin contractile stresses that drive flows in localized regions (20–23), leading to the formation of dynamic (nano-)clusters on the cell surface (7, 8). Predictions from this model have been verified in high-resolution fluorescence experiments in living cells (7, 8, 23) and in in vitro reconstitution of the active composite, viz actomyosin layered atop a planar bilayer membrane (19, 24).

The active nanoclustering appears to be a general phenomenon (3, 13); it is exhibited by transmembrane proteins that directly bind to actin, such as model proteins that consist of actin binding motifs at their cytoplasmic tails [transmembrane with actin binding domain (TMABD) (8)], and by naturally occurring proteins, such as E-Cadherin and CD44, that recruit actin binding modules to bind to cortical actin (10, 11). Further, lipid-tethered membrane proteins, such as outer-leaflet GPI-anchored proteins (GPI-APs) (7, 25, 26), glycolipids (12), and inner-leaflet Ras (27), also exhibit actin-dependent nanoclustering. While direct association with actin provides a mechanism for membrane molecules to couple to the actomyosin cortex, coupling between outer-leaflet GPI-APs or glycolipids and dynamic cortical actin filaments at the inner leaflet is mediated by transbilayer acyl-chain interactions involving long acyl chain–containing GPI anchors, inner-leaflet phosphatidylserine (PS), and cholesterol (28). Sphingolipids (SMs) have also been implicated in the maintenance of these nanoclusters (25). A necessary condition for the local stability of the transbilayer interaction at

Author contributions: S.S., A.D., S.M., and M.R. designed research; S.S., C.P., A.A.A., and P.S. performed research; S.S., C.P., and A.A.A. contributed new reagents/analytic tools; S.S., A.D., and C.P. analyzed data; A.D. and M.R. contributed theory and simulations; and S.S., A.D., S.M., and M.R. wrote the paper with inputs from all other authors.

Reviewers: P.B., Institut Curie; and J.F.J., Collège de France.

The authors declare no competing interest.

[1]S.S. and A.D. contributed equally to this work.

[2]Present address: Deputy Scientific Attaché, Embassy of France in India, Bangalore 560001, India.

[3]Present address: Department of Molecular Biology, Princeton University, Princeton, NJ 08544.

[4]To whom correspondence may be addressed. Email: mayor@ncbs.res.in or madan@ncbs.res.in.

This article contains supporting information online at https://www.pnas.org/lookup/suppl/doi:10.1073/pnas.2123056119/-/DCSupplemental.

Published July 22, 2022.

physiological temperatures was found to be the immobilization of PS at the inner leaflet together with the interdigitation of long acyl-chain lipids across the bilayer and the presence of adequate levels of cholesterol and SMs, predicting a nanoenvironment with local liquid order (lo) (28).

In this study, we use high-resolution fluorescence-based assays to study more closely the role of lipidic interactions, both transbilayer and lateral, in the active organization of the lipid-tethered GPI-AP and the transmembrane protein, TMABD (a schematic is in Fig. 1*A*). These observations provide the motivation for an active segregation model of a multicomponent fluid bilayer membrane comprising outer-leaflet GPI-AP, inner-leaflet PS, and lo- and ld-preferring lipids in both leaflets. We show that the combination of 1) active stress fluctuations arising from a coupling to cortical actomyosin, 2) a strong transbilayer interaction between PS and GPI/lo lipids, and 3) lateral lipidic interactions drives

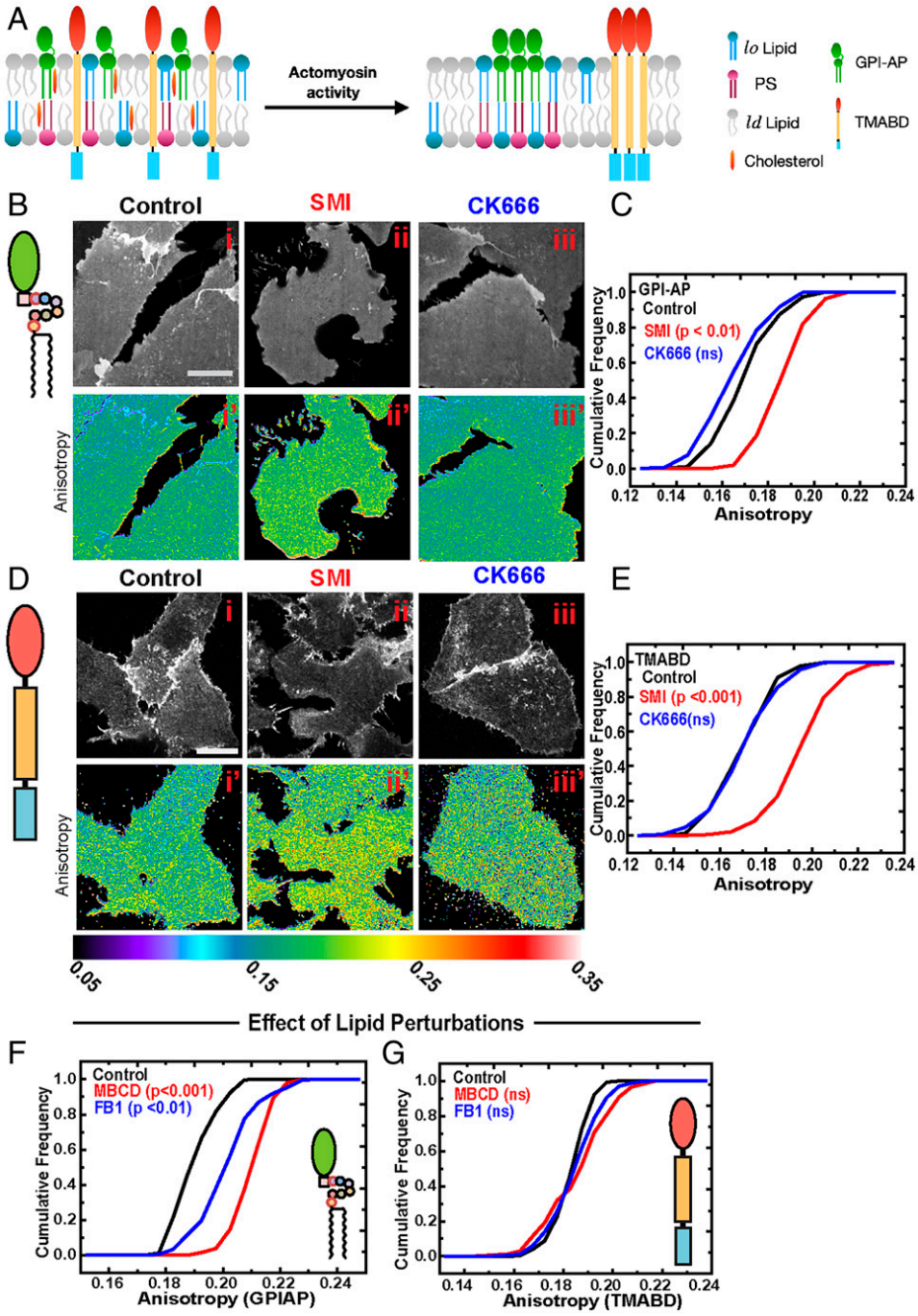

Fig. 1. GPI-AP and TMABD nanoclusters arise from different intermolecular interactions. (*A*) The schematic shows that actomyosin activity drives cell surface molecules, like GPI-AP and TMABD, into respective nanoscale clusters (*Right*). Note that while TMABD can directly couple to juxtamembrane f-actin, outer-leaflet GPI-APs can only do so via transbilayer coupling with inner-leaflet PS. (*B*–*E*) Representative confocal spinning disk images (*B* and *D*) showing fluorescence intensity (*B i–iii, D i–iii*) and anisotropy images (*B i'–iii', D i'–iii'*) of CHO cells expressing FR-GPI (*B*) or FR-TMABD (*D*) and labeled with PLB either untreated (control, *B i–i'* and *D i–ii'*) or treated with pharmacological inhibitors of formin (SMI, *B ii–ii'* and *D ii–ii'*) or Arp2/3 (CK666, *B iii–iii'* and *D iii–iii'*). Cumulative frequency plots (*C* and *E*) of anisotropy values from the indicated treatments show that formin perturbation (red lines) leads to significant ($P < 0.01$, KS test) increases in anisotropy of both FR-GPI and FR-TMABD, suggesting a reduction in nanoscale clustering, whereas Arp2/3 perturbation (blue lines) has no significant (using Kolmogorov-Smirnov [KS] test) effects on anisotropy. (Scale bars: *B* and *D*, 10 μm.) (*F* and *G*) Cumulative frequency plots of anisotropy values of CHO cells expressing EGFP-GPI (*F*) or FR-TMABD (*G*; labeled with PLB) from either untreated cells (control) or cells that were depleted of cholesterol (MBCD) or SM (FB1). Note that only GPI-AP anisotropy (but not TMABD) increases upon these perturbations. Data were pooled from at least 15 to 20 cells across independent replicates (2, 3) in each condition; statistical significance was tested with the two-sample KS test.

the mesoscale organization of GPI-APs at temperatures above the lo–ld phase segregation temperature. Such actively segregated mesoscale domains or active emulsions are expected to exhibit anomalous growth dynamics and fluctuations that are unique to the nonequilibrium steady state (29, 30).

To test these theoretical ideas, we use a combination of high-resolution maps of homo-Forsters Resonance Energy Transfer (FRET) (31) and local membrane order (32) to quantify the mesoscale organization of GPI-AP and TMABD nanoclusters and their correlation with the lipid environment. We find mesoscale domains of size $\approx 0.1\ \mu m^2$ enriched in GPI-AP nanoclusters, which in turn, coregister with inner-leaflet PS and are associated with higher lipid order, while mesoscale domains of TMABD nanoclusters are uncorrelated with lipid order. Importantly, disruption of key drivers of activity, viz the dynamic actin-filament nucleator formin, and mediators of GPI-AP binding to actin, viz transbilayer coupling of GPI-AP to PS, lead to a loss of lo-mesoscale domains. These results show how the interplay between active stresses (due to actomyosin contractility) and short-range passive forces (here represented by transbilayer coupling and weak lateral lipid–lipid interactions) provides the driving force for the formation of active emulsions at physiological temperatures, qualitatively and quantitatively consistent with predictions from our theoretical model.

Results

GPI-APs and Transmembrane Proteins Form Active Nanoclusters, Albeit with Different Intermolecular Interactions. In earlier studies, we and others showed that GPI-AP and TMABD form nanoclusters, which depend on dynamic cortical actin (7, 8, 25, 26, 33). Actin nucleation via formins but not Arp2/3 was identified to be involved in generating these filaments (23), which drive both steady-state and receptor signaling–triggered nanoclustering (34). Here, using homo-FRET imaging at high resolution to identify nanoclustering of fluorescently labeled proteins (31, 35), we confirm that GPI-AP and TMABD exhibit nanoscale clusters contingent on the same actin nucleator, formin, rather than Arp2/3 (34) (Fig. 1). Treatment of Chinese hamster ovary (CHO) cells expressing GPI-anchored folate receptor (FR-GPI) or folate receptor–tagged TMABD (FR-TMABD) labeled with $N\alpha$-pteroyl-$N\epsilon$-BodipyTMR-L-lysine (PLB) (8) with small molecule inhibitor of formin homology 2 domains [SMIFH2 (36)] but not inhibitors of Arp2/3 [CK666 (37)] disrupted the nanoscale clustering of both FR-GPI (Fig. 1*B* and *C*) and FR-TMABD (Fig. 1*D* and *E*). The cytoplasmic actin-filament binding domain (ABD) allows FR-TMABD to bind directly to actin (8). A single-point mutation in the cytosolic ABD (R579A; ABD*) abrogates actin binding and resulted in a complete loss of the formation of actin-driven nanoclusters (8).

The binding of GPI-AP is, however, indirect via a transbilayer coupling to PS at the inner leaflet and cytoplasmic actin (28). Consequently, perturbations of PS abrogate nanoclustering of GPI-APs (28) but not of FR-TMABD (38). Furthermore, depletion of cholesterol or SM levels abrogates the nanoscale organization of GPI-AP (Fig. 1*F* and *SI Appendix*, Fig. S1*A*) (23, 25, 39) but has no effect on the nanoclustering of TMABD (Fig. 1*G* and *SI Appendix*, Fig. S1*B*), consistent with the idea that both GPI-AP and TMABD engage with the active contractile machinery via distinct molecular interactions.

Theoretical Description of Active Segregation Involving Active Contractile Stresses and Transbilayer Coupling. These observations motivate a theoretical description of active segregation of the components of an asymmetric bilayer membrane that involves combining the nonequilibrium effects of actomyosin contractility with passive lipidic forces, namely the lateral interactions with lo-lipid components and transbilayer interactions with lower-leaflet PS (Fig. 2*A*).

Taking a coarse-grained view, we represent the asymmetric bilayer membrane by different components that include the primary players under discussion (*SI Appendix*, Fig. S2*A*)—1) GPI-AP in the upper leaflet; 2) the lo component in the upper leaflet comprising SM and cholesterol; 3) lower-leaflet PS together with other long-chain saturated lipids and cholesterol; the ld component in 4) the upper leaflet and 5) the lower leaflet comprising short chain or unsaturated lipids; and whenever applicable, a sixth component: 6) transmembrane protein TMABD. The membrane bilayer adjoins a layer of cortical actomyosin, which represents the source of the fluctuating active contractile stresses $\boldsymbol{\sigma}$ localized over a spatial scale ξ and a lifetime τ (8, 16, 18) and directly affects the lower-leaflet PS and the transmembrane TMABD, proportional to their binding affinity with cortical actin.

Here, we find it convenient to realize this active dynamics using a kinetic Monte Carlo simulation. A brief description of the active segregation in the asymmetric bilayer membrane with these components and their dynamics is presented in *Materials and Methods*, with further details in *SI Appendix* and *SI Appendix*, Fig. S2*A*. The transition rates associated with passive dynamics are determined from an energy function that depends on the short-range interaction potentials between the coarse-grained membrane components and obey detailed balance (*SI Appendix*, Fig. S2*A*). The transition rates associated with active dynamics correspond to two features first, the fluctuations of the active contractile stress represented by birth–death stochastic processes of contractile regions and second, centripetal contractile flows of PS and TMABD determined by local gradients of the active stress and violate the detailed balance (*SI Appendix*, Fig. S2*B*). These active transition rates depend on the following tunable parameters: 1) relative binding affinities of PS and TMABD to actin; 2) fluctuation statistics of the active contractile stress, viz the correlation length ξ and correlation time τ; 3) magnitude of contractile stress characterized by a Péclet number Pe or relative magnitude of active advective transport to diffusion outside; and 4) the extent of the activity or the fraction of the region influenced by active stresses. This generalizes a recent theoretical study (29, 30) of the coarse-grained dynamics of segregation of a two-component fluid driven by fluctuating active contractile stresses.

Our results (Fig. 2 *B*–*E*) show that a combination of active stress fluctuations and strong transbilayer coupling can induce mesoscale cosegregation of lo components, including GPI-APs, relative to ld components at a physiological temperature of 310 K, which is above the equilibrium lo–ld phase segregation temperature of 293 K determined empirically from giant plasma membrane vesicles (40). Fig. 2*B* shows a comparison between a typical snapshot of a steady-state configuration of the components in the absence of and with active contractile stresses at temperatures above the phase segregation temperature. The extent of segregation measured by the probability distribution of the segregation order parameter $P(\phi)$ (Fig. 2*C* and *D*) and their spatial profiles (Fig. 2*E*) depends on the binding affinity of PS with actin (Fig. 2*C*) and the strength of the transbilayer coupling (Fig. 2*D* and *E*).

The panels in Fig. 2*E* show the active cosegregation of the lo domains with GPI-AP in the upper leaflet of the membrane and their coregistry with PS in the lower leaflet. We see that the GPI-AP–enriched regions are predominantly surrounded by the lo component in the upper leaflet. The extent of segregation and coregistry increases with the affinity of PS to actin. The results on the active cosegregation of lo components and GPI-AP relative to

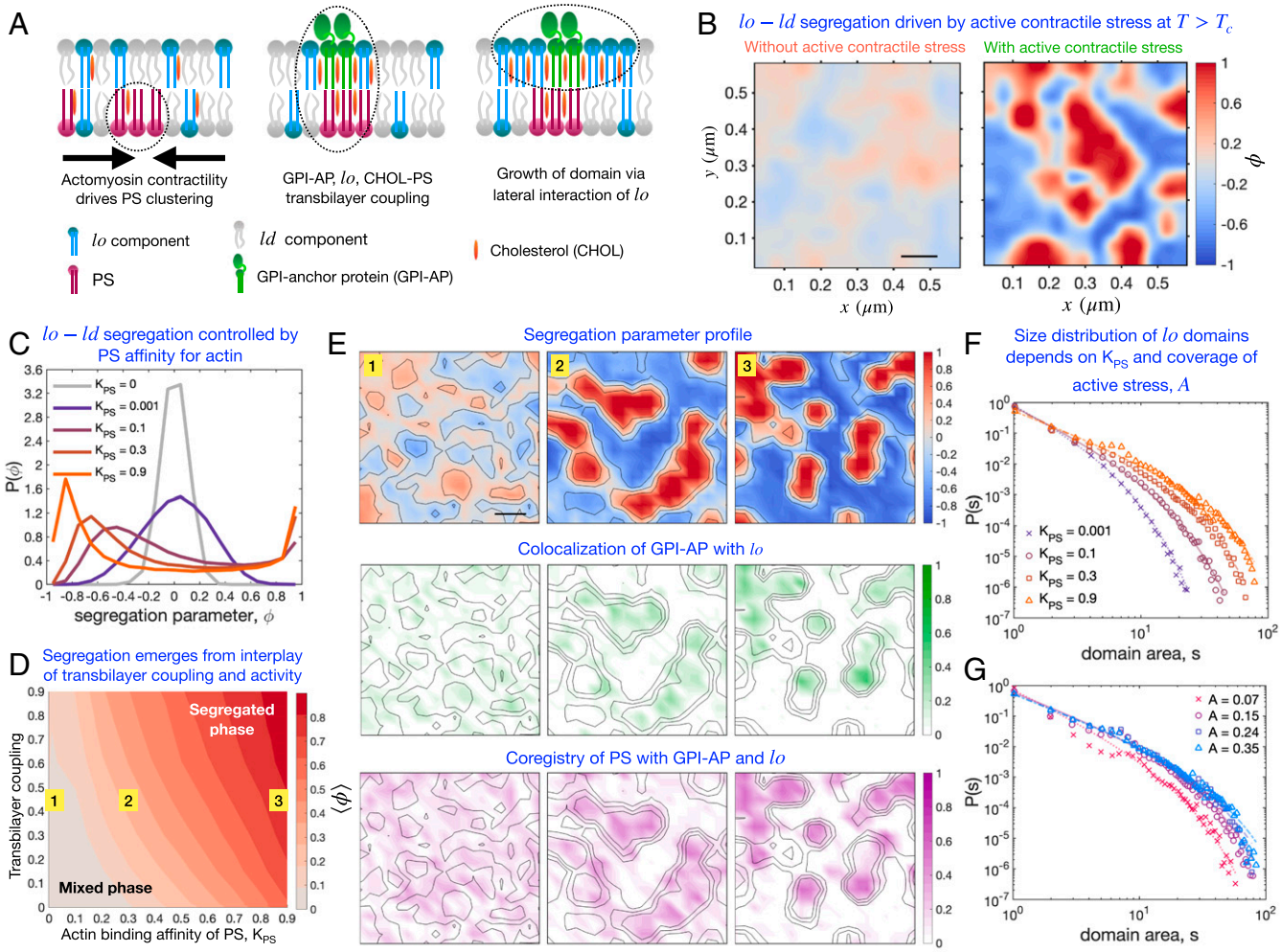

Fig. 2. Kinetic Monte Carlo simulation of a multicomponent model of an active composite cell surface predicts nano- to mesoscale lipid ordering and segregation of proteins driven by active contractile stresses generated by the actomyosin cortex. (*A*) Schematic of the three principal ingredients of the multicomponent model of the cell surface. For simplicity, we leave out showing the transmembrane protein TMABD, whose presence in the membrane does not make a qualitative difference to the GPI-AP–associated lo domains (*SI Appendix*, Fig. S2 has details). (*B*) Spatial profiles of the lo-ld segregation parameter ϕ (*Right*) in the presence of active contractile stresses and (*Left*) in their absence (all other parameters being fixed) at temperatures (T) higher than the critical temperature T_c of equilibrium lo-ld phase separation. ϕ is defined as $\phi = (\rho_{lo} - \rho_{ld})/(\rho_{lo} + \rho_{ld})$, where ρ_{lo} and ρ_{ld} are the local number densities of the lo and ld components, respectively. All simulation data correspond to $T = 1.05T_c$, close to the physiological temperature of the cell. (*C*) Dependence of the probability density functions of the segregation parameter ϕ on actin binding affinity of PS, K_{PS} (*SI Appendix, SI Text* has details). (*D*) Heat map of the order parameter, $\langle\phi\rangle$, as a function of the transbilayer coupling and K_{PS}. The angular brackets represent an average over multiple spatial locations and time frames. The transbilayer coupling is defined as the energy scale of PS (inner leaflet) - SM (outer leaflet) interaction U_{SM-PS} expressed in units of k_BT (Boltzmann constant k_B times the absolute temperature T). (*E*) Time-averaged spatial profiles of ϕ (*Top*) and number densities of GPI-AP (*Middle*) and PS (*Bottom*) at increasing K_{PS} (marked by numbers in *E*, *Top* and in *D*). In each case, the contours of ϕ are also shown as a guide. All the number densities are normalized by the maximum density possible on a grid point. (Scale bars: *B* and *E*, 0.1 μm.) (*F*) Distribution of the sizes of lo domains (s) with increasing K_{PS}. (*G*) Distribution of the sizes of *lo* domains (s) with increasing value of A, the area fraction of active contractile stress. In *F* and *G*, the solid lines are the fits to a model distribution, $As^{-\theta}\exp[-s/s_0]$. The values of fitting parameter A_0, exponent θ, and the cutoff s_0 are provided in *SI Appendix*, Table S1. Here, the unit of s is set by the unit grid area, which is 0.03 × 0.03 μm.

ld components continue to hold when an additional component, viz TMABD, is introduced, which only engages sterically with the other components but is driven by similar contractile stresses (*SI Appendix*, Fig. S2 *C* and *D*). The TMABD-enriched domains are segregated from lo domains and PS (*SI Appendix*, Fig. S2*E*).

The extent of mesoscale segregation and the mesoscale domains depend on the fluctuating active contractile stresses and appear at temperatures above equilibrium phase separation. Since the actomyosin-induced active stresses are contractile, localized regions of contractility will be drawn to each other depending on the gradient of contractile stress (21, 30). This paints a picture of an active emulsion driven by active stirring from the cortical medium, requiring inner-leaflet PS and outer-leaflet SM with cholesterol as a glue. While this is completely consistent with all our observations so far at the nanoscale, this description makes both qualitative and quantitative predictions about mesoscopic domains enriched in these nanoclusters, which we verify in experiments described below.

Evidence for Mesoscale Organization of GPI-AP Nanoclusters. A very clear prediction from the theoretical model is that GPI-AP nanoclusters will form mesoscale domains enriched in these entities. To explore the larger-scale organization of these nanoclusters, we repurposed our custom-built total internal reflection fluorescence (TIRF) and confocal spinning disk microscopes (31, 35) to obtain high-resolution spatial anisotropy maps of the labeled proteins over a scale of 300 to 1,000 nm. We identify optically resolvable domains enriched (or depleted) in these nanoclusters from spatial maps of fluorescence emission anisotropy (Fig. 3*A*) by thresholding the anisotropy at one SD from the mean (*Materials and Methods* and *SI Appendix*; the schematic is in *SI Appendix*, Fig. S3*A*). The thresholded anisotropy map of enhanced green

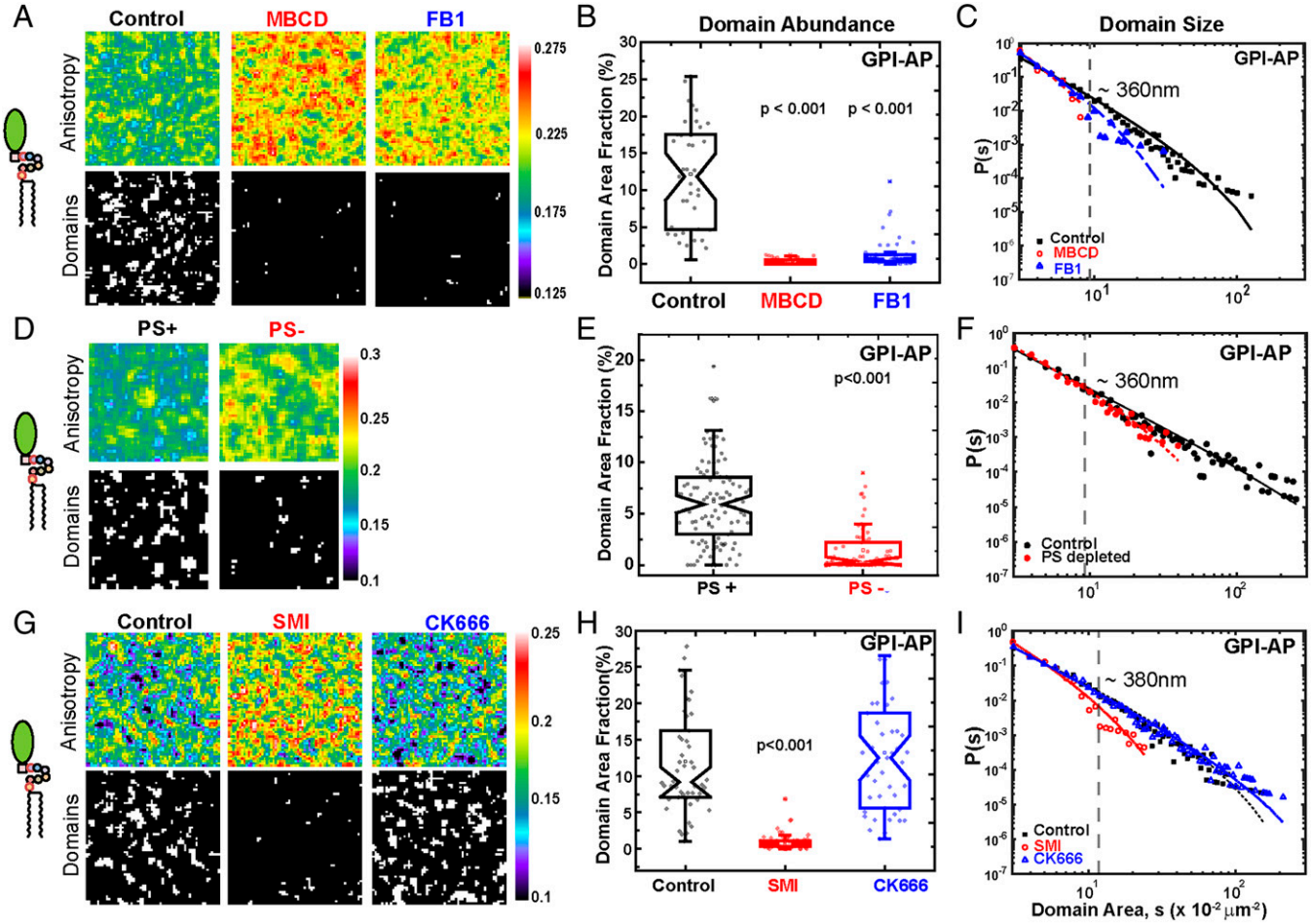

Fig. 3. Mesoscale organization of GPI-AP nanoclusters. (*A*) Boxes represent 6- × 6-μm patches of anisotropy map (*Upper*) and corresponding thresholded binary maps (*Lower*; showing mesoscale domains enriched in nanoclusters) taken from CHO cells expressing EGFP-GPI that were untreated (control) or depleted of cholesterol (MBCD) or SM (FB1). Notched box plots (*B*) of the domain area fraction obtained from several images like *A* show that mesoscale GPI-AP domains are significantly reduced upon these lipid perturbations ($P < 0.001$, one-way ANOVA with Tukey mean comparison). (*C*) Distribution of the domain area in the indicated conditions; the solid line represent the corresponding fits to a model distribution, $As^{-\theta}\exp[-s/s_0]$. The characteristic area of GPI-AP domains in the control scenario is estimated to be 0.1 μm^2 (dashed vertical line), which translates to a domain diameter of ≈360 nm, while both the lipid perturbations mark a shift toward smaller domain area as indicated by the decrease in the frequency $P(s)$ of larger domains ($s \geq 0.1$ μm^2). (*D–F*) PS-deficient PSA3 cells transiently expressing EGFP-GPI were grown in PS+ or PS− conditions. Anisotropy and binary domain maps (*D*; 6-μm × 6-μm boxes) show that PS depletion led to a reduction in the domain area fraction (*E*; $P < 0.001$, Mann–Whitney test), and domain area distributions (*F*) show a shift toward smaller domain areas for PS-depleted cells (red circles and the dotted fit line). (*G–I*) Boxes (*G*) show 6 × 6 μm anisotropy and binarized domain maps of PLB-labeled FR-GPI obtained from untreated cells (control) or cells treated with inhibitors of formin (SMI) or Arp2/3 (CK66). The notched box plot (*H*) of the domain area fraction shows that only formin perturbation leads to loss of these domains and led to a marked shift to smaller s in domain area distributions (*I*). Statistical significance was determined at $P < 0.001$ using one-way ANOVA with Tukey mean comparison. At least 30 to 60 thresholded binary maps were pooled from 10 to 15 cells across two independent replicates for the analyses of each condition.

fluorescent protein (EGFP) tagged GPI (EGFP-GPI) (Fig. 3*A*) or FR-GPI bound to fluorescent ligands (*SI Appendix*, Fig. S3*B*) shows a nanocluster fraction in excess of ≈10 to 15% of the mapped area and mean domain area ≈0.1 μm^2 (control in Fig. 3*B* and *C*), consistent with previous work (7). The dependence of GPI-AP nanoclustering on adequate levels of cholesterol and SM is consistent with their depletion severely perturbing the mesoscale domains (Fig. 3*A–C*). The mesoscale domains of GPI-APs are also lost when the levels of the transbilayer coupling lipid, PS, were perturbed in CHO cells deficient in phosphatidylserine synthase 1 (PSS1) activity and were grown in the absence of ethanolamine to reduce membrane PS levels (28) (Fig. 3*D* and *E*). As predicted, the thresholded anisotropy map of TMABD also shows mesoscale domains where the nanocluster fraction is in excess of ≈ 10% of the mapped area and a mean domain area ≈0.1 μm^2 (*SI Appendix*, Fig. S3 *E*, *F*, *H*, and *I*). In contrast to the GPI-APs, the mesoscale organization of TMABD is unaffected by the lipid perturbations (*SI Appendix*, Fig. S3 *E* and *F*). However, it is much reduced upon abrogation of the actin binding capacity (*SI Appendix*, Fig. S3 *H* and *I*).

Since formin-nucleated dynamic cortical actin is necessary for building the nanoscale clusters of GPI-AP and TMABD (34), formin inhibition also leads to a significant reduction in their mean domain area (Fig. 3*G* and *H* and *SI Appendix*, Fig. S3 *K*, SMI, and *L*, SMI), whereas Arp2/3 perturbation does not alter these parameters (Fig. 3*G* and *H* and *SI Appendix*, Fig. S3 *K*, CK666, and *L*, CK). These results confirm the qualitative predictions of the creation of mesoscale domains of nanoclusters driven by contractile stresses in two distinct classes of molecules: GPI-APs linked via the virtue of the local lipid environment and the TMABD to dynamic cortical actin.

Mesoscale Domain Size Distributions Are Sensitive to Actin Binding Affinity and Cortical Actin Dynamics. A quantitative prediction of the theory, as elaborated previously (29), is that as a consequence of active driving, the steady-state domain size

distribution $P(s)$ scales as $s^{-\theta}\exp(-s/s_0)$, a power law with an exponential cutoff at $s = s_0$ (Fig. 2*F* and *G*). The exponent θ and the cutoff scale s_0 depend on the actin binding affinity, the extent of activity, and correlation time τ of the active stress fluctuations (Fig. 2*F* and *G*). Using the spatial maps of the steady-state fluorescence anisotropy of GPI-AP and TMABD, this domain size distribution is easily measured. We find a good fit of the mesoscale domain size distribution data to the predicted form of $P(s)$, with $\theta \approx 2$ and $s_0 \approx 0.4$ to $0.7\ \mu m^2$, for both GPI-AP (Fig. 3*C*, *F*, and *I*) and TMABD (*SI Appendix*, Fig. S3 *G*, *J*, and *M* and Table S1).

The steady-state distribution of cluster sizes still retains the above form upon perturbations of the actomyosin dynamics and the actin binding affinity, albeit with different values of θ and s_0. Based on our earlier study of active segregation (29) and the predictions from the current model, s_0 should always decrease with any of the above perturbations. This is consistent with what we observe in our perturbation experiments (Fig. 3 and *SI Appendix*, Fig. S3 and Table S1).

Together, these data show that the two types of membrane components, GPI-AP and TMABD, both actively driven by cortical actin-based machinery (formin-nucleated filaments) inhabit mesoscopic membrane domains with distinct characteristics, consistent with our predictions.

Mesoscale Domains of GPI-AP Are Correlated across the Bilayer with PS and with lo Regions. The active emulsion picture suggests that the mesoscale organization of nanoclusters of outer-leaflet GPI-AP is contingent on coregistry with nanoclusters of PS at the inner-leaflet and lo regions (schematics are in Fig. 4*A*

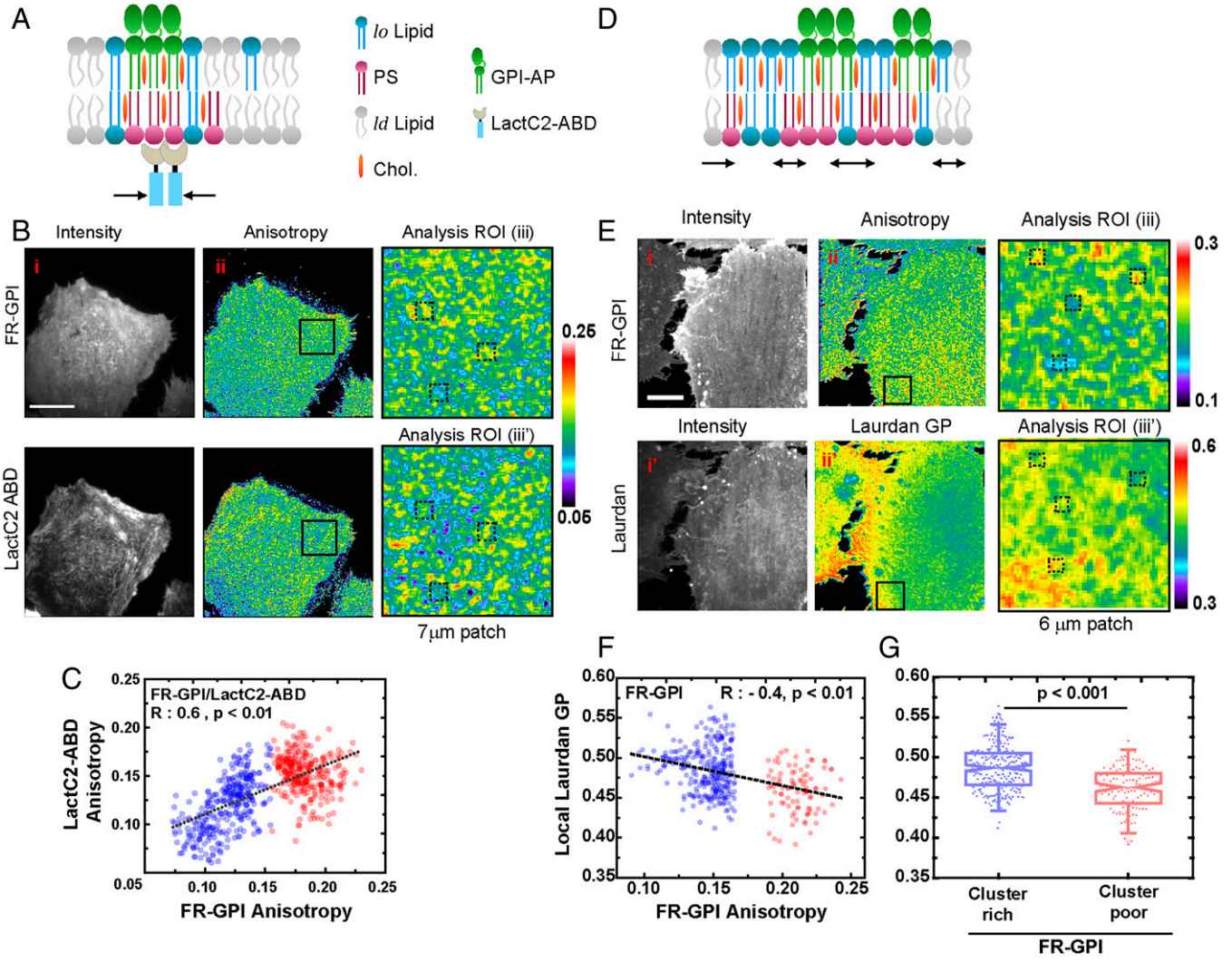

Fig. 4. Mesoscale domains of GPI-AP clusters are correlated with inner-leaflet PS cluster-rich and lo domains. (*A*) The schematic shows transbilayer coupling between the GPI-AP and inner-leaflet PS. LactC2-ABD acts as a synthetic linker between the inner-leaflet PS and juxtamembrane actin flows (black arrows). Representative TIRF images of fluorescence intensity and anisotropy of PLB-labeled FR-GPI (*B*, *i–iii*) transfected with YFP-LactC2-ABD (*B*, *i'–iii'*). Matched ROIs of 7×7 μm-sized patches (black boxes in *B*, *ii*) were chosen from the anisotropy images of PLB-labeled FR-GPI and LactC2-ABD (*B*, *iii* and *iii'*). Mesoscale domain–sized ROIs (≈400 × 400 nm) are drawn around cluster-rich and cluster-poor hot spots of FR-GPI (*B*, *iii* and *iii'*). The anisotropy values of FR-GPI and LactC2-ABD graphed as scatterplots (*C*) exhibit significant positive correlation (Pearson's $R = 0.6$, $P < 0.001$). Individual scatterplots report 630 ROIs collected from cells ($n = 29$ cells) pooled from two independent replicates. (*D–G*) The schematic (*D*) shows how individual nanoscale GPI-AP clusters cohabit a larger mesoscopic patch of lo-like membrane driven by actin flows to form "active emulsions." Representative high-resolution confocal fluorescence and anisotropy images show CHO cells expressing FR-GPI labeled with PLB (*E*, *i–iii*) and colabeled with the membrane order probe, Laurdan (*E*, *i'–iii'*). Identical 7×7 μm-sized boxes (in black) were chosen from the anisotropy and Laurdan GP map and are shown in analysis ROIs (*E*, *iii* and *iii'*, respectively). (Scale bars: *B* and *E*, 10 μm.) A scatterplot (*F*) of local Laurdan GP and anisotropy computed from corresponding small regions (400 × 400 nm; dashed boxes in *E*, *iii* and *iii'*) obtained from analysis ROIs for corresponding FR-GPI anisotropy (*E*, *iii*) and Laurdan GP (*E*, *iii'*) maps. Note that Laurdan GP and anisotropy of PLB-labeled FR-GPI show negative correlation ($R = -0.4$, $P < 0.01$). (*G*) Box plots show that cluster-rich domains of GPI-AP have significantly higher local Laurdan GP ($P < 0.001$, two-sample Student's *t* test). Datasets (*F* and *G*) report on at least 500 ROIs collected from cells ($n = 15$ cells) pooled from two independent replicates.

and *D*). To study the correlation of mesoscale domains with other membrane components, we developed a two-color emission anisotropy (homo-FRET) methodology, wherein we image two different components in the same cell membrane in a sequential fashion (*SI Appendix*, Fig. S4 *A–E*). To examine coregistry with inner-leaflet nanoclusters of PS, we built a fusion protein of PS binding the discoidin-like C2 domain of lactadherin (LactC2) in tandem with ABD of Ezrin and yellow fluorescent protein (YFP) (YFP-LactC2-ABD). This fusion protein was designed to be recruited to the inner-leaflet PS (41) and connect to the dynamic cortical actin machinery via its Ezrin–actin binding domain (28). LactC2-ABD-YFP forms nanoclusters at the inner leaflet as indicated by its depolarized emission anisotropy and subsequent increase upon photobleaching (*SI Appendix*, Fig. S4*F*) (25). To visualize the nanocluster-rich regions of GPI-AP and PS in the same cells, we transfected YFP-LactC2-ABD–encoding plasmids in FR-GPI–expressing cells and labeled FR-GPI with a fluorescent folate analog (PLB). We confirmed by sequential imaging of anisotropy of individual components that LactC2-ABD-YFP and PLB-labeled FR-GPI coexisted in highly correlated regions (*SI Appendix*, Fig. S4 *D*, *E*, and *G*). Analysis of the correlation of the spatial anisotropy maps of the outer- and inner-leaflet localized proteins (Fig. 4*B*) showed that the cluster-rich (low-emission anisotropy) regions of the LactC2-ABD are strongly correlated with the cluster-rich regions of GPI-AP (Pearson coefficient = 0.6, $P < 0.01$) (Fig. 4*C*) but only moderately with TMABD (Pearson coefficient = 0.28, $P < 0.01$) (*SI Appendix*, Fig. S4 *H* and *I*). Together with our previous findings (28), this shows that the actively generated mesoscale organization of GPI-AP nanoclusters occurs at sites of enrichment of PS clusters in the inner leaflet mediated by transbilayer coupling, as predicted by the theory.

Next, we sought to understand the local lipid order of these cluster-rich (or sparse) mesoscopic domains of FR-GPI. To do so, we map local membrane order using the polarity-sensing lipid probe 6-lauryl-2-dimethylamino-napthalene (Laurdan) and quantify it by measuring generalized polarization (GP) (42–44). GP values are lower in ld regions and higher in lo regions of the membrane. While the dynamic range of the Laurdan GP values in CHO cells is not very large, as has been noticed in earlier cellular studies (45) and in cell-derived giant plasma membrane vesicles (46), it is sufficient to identify regions enriched in lo or ld components.

We obtained sequential spatial maps of Laurdan GP and emission anisotropy (homo-FRET) of GPI-AP using a spinning disk confocal microscope on a uniformly labeled basal membrane (Fig. 4*E* and *SI Appendix*, Fig. S5 *A–D*). We measured the anisotropy coarse grained over 4×4 pixels (pixel: 102 nm) and determined the cluster-rich (cluster-sparse) regions together with the corresponding Laurdan GP from membrane patches across multiple cells (Fig. 4*E*). We found that GPI-AP nanocluster-rich domains have a higher Laurdan GP compared with GPI-AP nanocluster-poor domains (Fig. 4*F* and *G*). On the other hand, the TMABD cluster-rich (or sparse) regions have very little difference in their local membrane order (*SI Appendix*, Fig. S5 *E–G*). These results suggest that mesoscale domains enriched in GPI-AP nanoclusters have a specific lo-lipid environment, while the TMABD nanoclusters are agnostic to its lipid environment, exactly as predicted by our theory.

Lateral Membrane Ordering Is Contingent on Dynamic Cortical Actin and Transbilayer Coupling. An important claim of the active emulsion description is that the mesoscale lo region observed at physiological temperatures is not a consequence of a thermodynamic phase transition but rather, driven by active contractile stresses arising from cortical actomyosin that act via the inner-leaflet PS to maintain a strong transbilayer coupling to GPI-AP. To test this crucial prediction, we study how local membrane ordering, characterized by Laurdan GP, gets affected upon perturbing the actin nucleator formin, actin (de-)polymerization, and inner-leaflet PS.

Perturbations of formin (SMIFH2, 25 μM, 2 h) but not Arp2/3 (CK666, 50 μM, 2 h) led to a reduction in GP values on CHO cells as measured using two different probes for membrane ordering, viz Laurdan (Fig. 5) and the outer leaflet–specific Nile Red analog NR12S (47, 48) (*SI Appendix*, Fig. S6). Treatment of cells with formin inhibitor, SMIFH2 (Fig. 5*A*, SMI) led to a significant reduction in steady-state Laurdan GP and NR12S ratios (Fig. 5*A* and *B* and *SI Appendix*, Fig. S6 *A*, SMI, and *B*, SMI). However, treatment with Arp2/3 inhibitor does not affect the Laurdan GP or NR12S ratios compared with control (Fig. 5*A* and *B* and *SI Appendix*, Fig. S6 *A*, CK666, and *B*, CK666). Finally, Latrunculin A (Lat A)–mediated inhibition of actin polymerization in general (Fig. 5*A*, Lat A, and *B*, Lat A) also lowers GP value. Note that for the NR12S probe, the shift in GP values is small but statistically significant (*SI Appendix*, Fig. S6 *A*, Lat, and *B*, Lat A). Laurdan GP measured from PS-deficient cells (PS−) shows a clear drop in steady-state membrane order in comparison with cells grown in the presence of ethanolamine (PS+ in Fig. 5*C* and *D*). The extent of decrease in Laurdan GP in PS− cells is comparable with that obtained from PS+ cells depleted of cholesterol (PS+ [+methyl-β-cyclodextrin (MBCD)] in Fig. 5*C* and *D*), buttressing the critical role of inner-leaflet PS in maintaining local membrane order. Not surprisingly, the depletion of membrane cholesterol (MBCD) and outer-leaflet SM (by treatment with fumonisin B1 [FB1]) in wild-type cells also show marked reduction in membrane ordering (Fig. 5*E* and *F*).

These observations verify a critical aspect of the theory, namely that the concerted involvement of dynamic cortical actin and transbilayer interaction via inner-leaflet PS drives the local lo-membrane order that accompanies the mesoscale organization of GPI-AP nanoclusters.

Discussion

Several studies lend support to the picture of the cell surface as a multicomponent composite—an asymmetric bilayer membrane sandwiched between a thin cortical layer of actomyosin and an extracellular matrix (49). The membrane itself has rich compositional diversity, consisting of a variety of lipids and proteins. In this context, many transmembrane protein receptors have evolved intracellular domains, allowing them to interact with the cortical cytoskeleton either directly or via recruiting actin binding domains, such as Ezrin, ankyrin, or α-catenin (50, 51). This interaction, where analyzed, depends on formin-nucleated cortical actin (10, 11). On the other hand, proteins and lipids localized to the outer leaflet of the plasma membrane, such as the lipid-tethered GPI-APs and glycolipids, also interact with formin-nucleated cortical actin, albeit in an indirect manner. Their interaction is mediated via the creation of a specific lo-lipid environment at nanoscales, involving acyl-chain transbilayer coupling with inner-leaflet PS and the stabilizing influence of local cholesterol and SM (12, 28).

The active composite membrane model elaborated here describes the dynamical response of GPI-APs (and possibly, glycolipids) at the outer leaflet as a consequence of being internally driven by active actomyosin-dependent stresses. As we show here, it predicts that these nanoclusters are organized in mesoscale domains that exhibit lo characteristics. Validating these predictions,

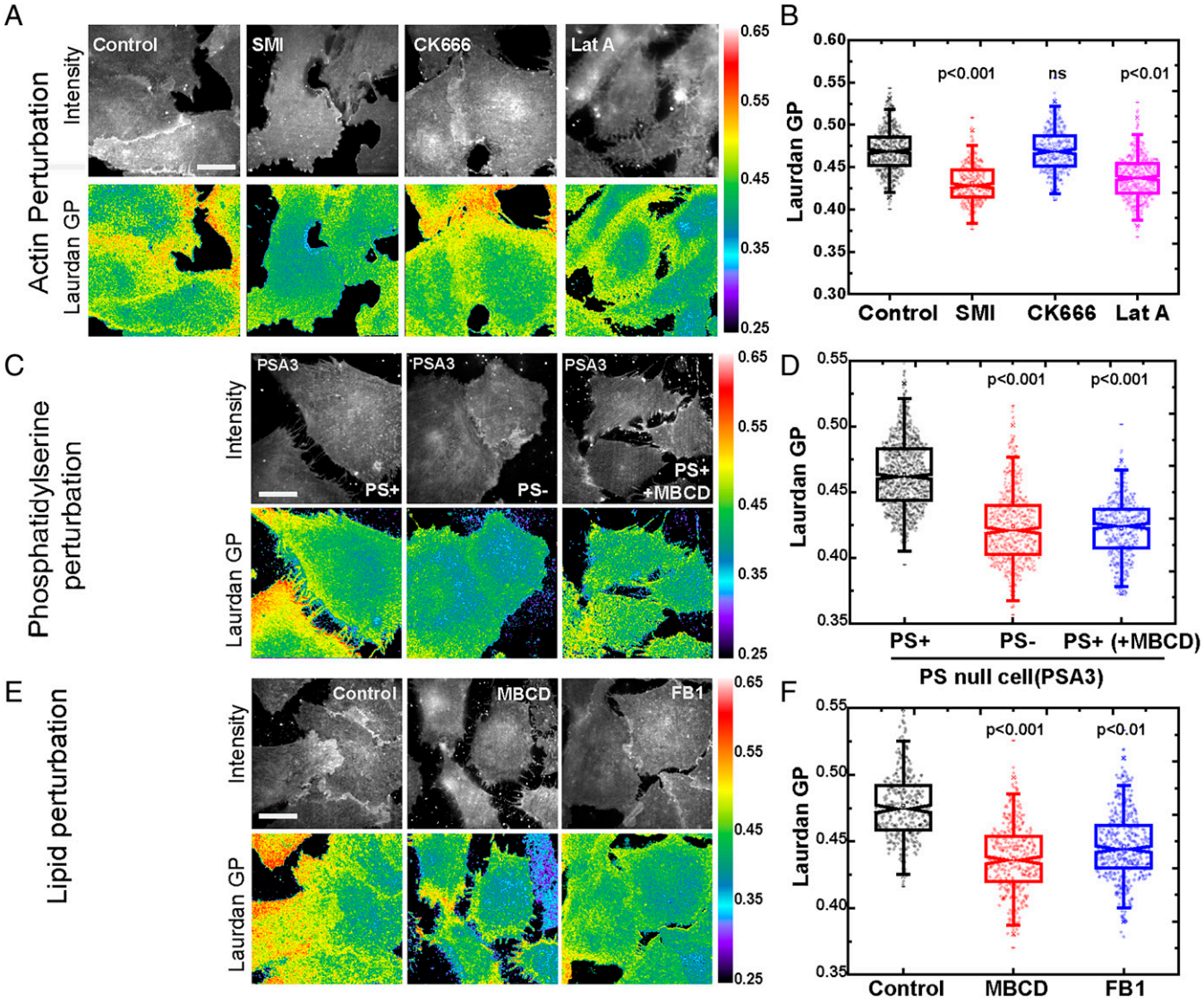

Fig. 5. Molecular components driving the formation of ordered domains. (*A* and *B*) Representative confocal images (*A*) show Laurdan total intensity (intensity) and GP maps of untreated CHO cells (control) or cells treated with different perturbation of actin cytoskeleton. (*B*) The box plot shows the effects of different actin perturbations on Laurdan GP. Perturbation of actin polymerization (Lat A; pink) or formin (SMI; red) but not Arp2/3 (CK666; blue) leads to significant reduction of Laurdan GP compared with control (black). (*C* and *D*) Laurdan intensity and GP images (*C*) of the PS biosynthetic mutant CHO cells (PSA3) grown in the presence (PS+) or absence (PS−) of ethanolamine. The box plot (*D*) shows that Laurdan GP of PS− (red) cell membrane is reduced significantly compared with PS+ (black), suggesting a reduction of steady-state membrane ordering. Cholesterol depletion of PS+ cells by MBCD (*C* and *D*, blue) leads to similar loss of membrane ordering. (*E* and *F*) Representative confocal images (*E*) of CHO cells show Laurdan intensity and GP maps of untreated cells (*E*, control) or cells depleted of cholesterol (MBCD) or SM (FB1). (Scale bars: *A*, *C*, and *E*, 10 μm.) (*F*) The box plot of Laurdan GP shows the reduction of membrane ordering in cholesterol (red)- and SM (blue)-depleted cells compared with control (black). The dataset for each condition was collected from at least 300 to 500 regions (individual dots in box plots) from 15 to 20 cells pooled from two independent replicates. Statistical significance was defined at $P < 0.001$ using one-way ANOVA with the Tukey mean comparison test.

we find mesoscopic domains enriched in clusters whose size is ≈350 to 500 nm, consistent with earlier high-resolution studies (7, 33, 52). This lateral mesoscale organization of nanoclusters is contingent on 1) transbilayer coupling to inner-leaflet PS; 2) the binding of PS to the active machinery and consequently, subject to active contractile stresses; and 3) the presence of lo-lipid components, such as SM and cholesterol. As a consequence, this lateral organization manifests at physiological temperatures, which are significantly higher than the thermodynamic lo–ld phase transition. As confirmed in experiments, the lo domains are dependent on a dynamic actin cortex comprising formin-nucleated actin filaments.

Fig. 6 shows a schematic of the emergence of this mesoscale organization driven by active contractile stresses, transbilayer coupling via PS, and lateral lipidic interactions. This preexisting lateral segregation on the flat asymmetric bilayer cell membrane is aptly described as an active emulsion formed by local nonequilibrium stirring of the composite. We expect such active emulsions to display anomalous fluctuations in their nonequilibrium steady state (24, 30). This description differs from passive (micro-) emulsion models, such as those that invoke preferential wetting as in the lipid–shell model (5) or that impute line actants (53, 54) or depend on the coupling of membrane shape fluctuations to local lipid composition (55, 56), in two fundamental aspects. First, there is an identification of a previously unappreciated molecular organizer of local plasma membrane composition, namely cortical actomyosin and its linkage to the lower-leaflet lipid PS, along with attendant lateral interactions. Second, it is dependent on hitherto unnoticed forces for driving local organization, namely nonequilibrium active contractile stresses and passive

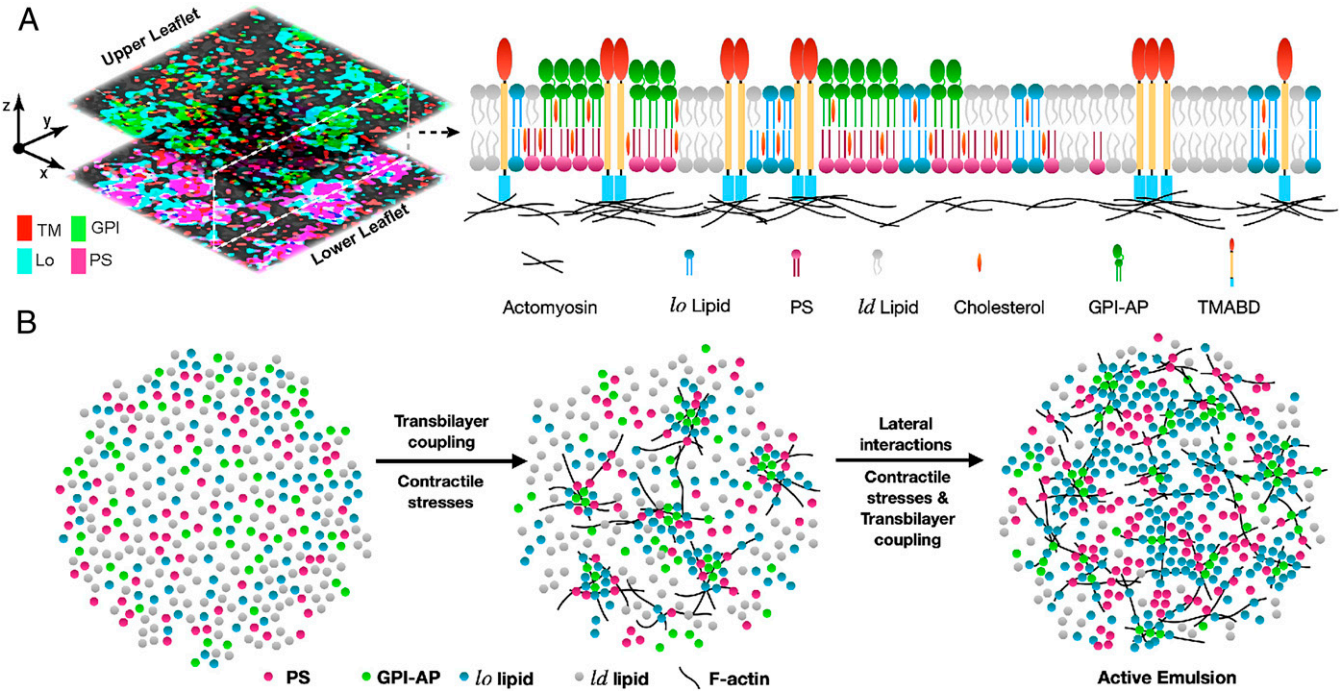

Fig. 6. Active emulsions: emergent mesoscale domains at the cell surface. (*A*) The image (*Left*) shows a spatially averaged map of upper- and lower-leaflet components obtained from a snapshot of simulations described in Fig. 2. Here TM represents a generic transmembrane protein with actin binding capacity. An axial slice (*Right*) of the cell membrane schematizes the organization of the resultant patches of GPI-AP clusters enriched in lo-membrane components and juxtamembrane actin interactions at the inner leaflet. (*B*) Model for the emergence of active emulsions. Transbilayer coupling and contractile stresses organize GPI-APs and lo lipids present in a uniformly mixed bilayer (*Left*) to form an individual nanoscale cluster (*Center*), which in turn, sets up the platforms to facilitate local lipid–lipid lateral interactions leading to the emergence of ordered mesoscopic domains or active emulsion (*Right*).

transbilayer interactions. It is the combination of active internal forces driven by a molecular mechanism involving actomyosin and specific passive interactions, including transbilayer interaction with PS and lateral interaction with lo components, that outcompetes the entropy of mixing and drives lateral organization of lipids at the nano- and mesoscales in the plasma membrane at physiological temperatures.

Concurrently, the lateral active organization of transmembrane proteins, such as TMABD, that bind directly to actin appears to be agnostic of the underlying membrane composition. Their mesoscale organization arises from a combination of active internal forces driven by actomyosin and passive protein–protein interactions. This may provide an explanation for the mesoscale domains of several actin-interacting endogenous proteins, which also exhibit cisinteractions in their ectodomains, such as CD44 and E-Cadherin (10, 11, 57). In the event that there are covalent or noncovalent interactions of these proteins with specific lipids that prefer lo or ld phases, we propose that such actively driven protein clusters will also be correlated with specific lipid environments, dictated by these interactions.

The active emulsion picture elucidated here has parallels in the creation and maintenance of liquid–liquid phase-separated assemblies (58, 59), otherwise known as biomolecular condensates (60). Apart from purely thermodynamic agencies driving such biomolecular aggregation (58–60), it is likely that activity, arising from either nonequilibrium chemical reactions (61) or active cytoskeletal elements (as discussed here), could provide the driving force for the formation and maintenance of such mesoscale emulsions.

The preexisting dynamic organization of the plasma membrane described here is maintained out of equilibrium by constitutive active processes. This active nonequilibrium steady state sets up the plasma membrane to respond sensitively to stimuli, such as in outside-in and inside-out cell surface signaling (18). It is, therefore, no surprise that many membrane signaling receptors have evolved intricate direct or indirect molecular mechanisms linking them to the cytoskeleton (10, 11, 57, 62).

For instance, the hierarchical architecture of having mesoscale domains of membrane proteins, built from dynamic nanoscale motifs, allows for a rapid remodeling of an activated zone (13, 18, 22). The strength and nature of the coupling between the actomyosin machinery and membrane components could be locally regulated to build larger platforms or disassemble existing ones. A striking example of this is the rapid expansion of an activated zone of GPI-AP nanoclusters induced during local integrin activation and cell substrate adhesion, with consequences for cell physiology and receptor function (34).

Finally, there are two immediate and important consequences of the induced and preexisting active organization of membrane components. One is the central involvement of actomyosin in nano- and mesoscale organization. This allows the cell to explore mechanochemical mechanisms for the local control of cell membrane organization and thereby, mechanochemical signal processing and feedback (63, 64). The second is the key finding of differential segregation of membrane components driven by active contractile stresses. This must direct the focus to uncovering the molecular basis of active contractile force generation at the cortex—their chemistry and interaction partners, force characteristics, spatial organization, and turnover.

Materials and Methods

Cell Lines, Labeling, and Perturbation. CHO cell lines were maintained in Ham's F-12 media (Hi Media) supplemented with (10%) fetal bovine serum (FBS; Gibco). Plasmids were either expressed stably (FR-GPI, FR-TMABD, EGFP-GPI) or transiently transfected (LactC2-ABD-YFP) prior to imaging. The PSA3 cell line for PS perturbation experiments was maintained in Ham's F-12 medium in the presence of 10 mM ethanolamine and 10% FBS. PLB was used to label

folate receptor (FR-GPI and FR-TMABD)–expressing cells at saturating concentration (∼400 nM) for 5 min at 37 °C. Imaging was carried out in a HEPES (20 mM)–based buffer supplemented with 2 mg/mL glucose (details are in *SI Appendix, Supplementary Methods*).

Perturbations were carried out as follows: 1) cholesterol: MBCD; 10 mM at 37 °C for 30 min; 2) SM: FB1; 40 μg/mL for 72 h in growth culture media; 3) PS depletion: PSA3 cells were grown in media devoid of ethanolamine and 10% dialyzed FBS for 36 to 48 h; 4) F-actin: Lat A; 2 μM for 10 to 15 min at 37 °C; 5) formin: SMIFH2; 25 μM for 2 h at 37 °C; and 6) Arp2/3: CK666; 50 μM for 2 h at 37 °C. Unless noted otherwise, the drugs against F-actin, formin, and Arp2/3 were maintained in the imaging buffer during microscopy.

Steady-State Anisotropy Measurements. Steady-state anisotropy experiments were carried out as described earlier (31, 35) using the following high-resolution (100× objective, 1.45 NA) imaging platforms: 1) Yokogawa CSU-22 spinning disk confocal microscope (Andor Technologies; with a sampling pixel size of 100 nm) or 2) Nikon TIRF microscope (with a pixel size of 75 nm). Image processing, analysis, and quantification were performed using Metamorph 7.0 (Molecular Devices Corporation), MATLAB (MathWorks), and ImageJ (NIH) as described earlier and detailed in *SI Appendix*.

Membrane Ordering Measurements. Membrane ordering measurements were primarily carried out by measuring the GP of Laurdan at the cell surface. Cells were colabeled with Laurdan (at 10 μM) and the folate analog PLB (at 400 nM) at 37 °C for 5 min. Laurdan-labeled cells were imaged at 100× (1.45 numerical aperture [NA]) on a confocal spinning disk microscope using 405-nm laser line, and emission fluorescence was recorded at the two spectral channels 410 to 460 nm (Ch1) and 470 to 530 nm (Ch2). Laurdan GP calculation and standards were implemented as described earlier and detailed in *SI Appendix* (32, 43).

In some experiments, Nile Red–based membrane dye (NR12S) blue–red ratiometric imaging provided an alternate measure of lipid order (48) as detailed in *SI Appendix*.

Image and Data Analysis.

Quantification of domain abundance and size distributions. Pixel anisotropy distribution obtained from several (20) 6- to 10-μm square patches of spatial anisotropy maps of a probe (say FR-GPI in control conditions) was used determine the mean and SD and set the threshold (mean–SD). Mesoscopic domains were demarcated by thresholding and binarizing spatial anisotropy maps. For comparisons between control and perturbations, the same threshold determined from "control" was used uniformly across all conditions. These binarized maps were quantified using the "Analyze particles" routine of ImageJ with a size criterion of at least five pixels (pixel size is 0.1 μm or area of 0.01 μm^2) to obtain the domain area fraction (for each patch) and individual domain area.

Quantitative relation between clustering (of two probes) and with lipid order. A systematic correlation-based approach was implemented to compute the relation between the clustering (from anisotropy values) for two probes or that between clustering and lipid order (Laurdan GP). Briefly (details are in *SI Appendix*), anisotropy-rich and -poor regions were manually identified (say for FR-GPI; probe 1) and demarcated with a region-of-interest (ROI) box surrounding the domains. The size of the box (0.4 × 0.4 μm; 0.16 μm^2) was guided by the mesoscopic domain sizes we determined earlier, and several ROIs (at least 300 to 500) were marked across the entire dataset (at least 15 cells across two to three independent replicates). These ROIs were then used to calculate anisotropy values of both probes (say FR-GPI and LactC2-ABD) or anisotropy of a given probe (FR-GPI) and its corresponding GP values from Laurdan maps. The data were displayed as scatterplots to show the qualitative trend of correlation and compute the Pearson's correlation coefficient.

Theory and Simulation. We briefly present a theoretical description of active-phase segregation in a multicomponent asymmetric bilayer membrane driven by the combination of active contractile stresses and the passive lipidic forces, namely transbilayer coupling and lateral interactions. A more detailed account of the kinetic Monte Carlo simulation is provided in *SI Appendix*, *SI Text* and Fig. S2.

Coarse-grained multicomponent asymmetric bilayer. The asymmetric bilayer comprises at least five components, $\alpha = 1, \ldots, 5$, as described in Fig. 2*A*. In the cases where we compare the organization of GPI-AP with a generic transmembrane protein (TMABD) that can bind to cortical actin, we include one more component, $\alpha = 6$. We represent all molecules as coarse-grained spheres of equal size σ, residing either on the upper or lower leaflet of the bilayer or both (as in the lo and ld components).

A pair of lo, a pair of ld, and a GPI-AP and lo component on the same leaflet interact via the Lennard–Jones attractive potential (*SI Appendix*). Components residing on different leaflets do not have to interact sterically. Only PS or lo on the lower leaflet and lo or GPI-AP on the upper leaflet interact via transbilayer coupling, which is represented by the same attractive potential mentioned above. The TMABD being transmembrane has just steric interactions with components on either leaflet.

Active contractile stresses from actomyosin cortex. The cortex is a viscous gel (thin film) that gives rise to fluctuating active contractile stresses with nonzero spatial average and whose spatiotemporal correlations are

$$\langle \boldsymbol{\sigma}(\mathbf{r}, t)\, \boldsymbol{\sigma}(\mathbf{r}', t') \rangle = f(|\mathbf{r} - \mathbf{r}'|/\xi)\, g(|t - t'|/\tau),$$

where we have suppressed the tensor indices. The functions f and g are sharply decaying functions (e.g., bump functions or exponentially decaying functions). Such active contractile stress fluctuations have been studied in refs. 65–67 and can be dynamically realized using a birth–death process of contractile stress events localized over a region ξ with a lifetime τ (18, 29, 30).

The cortical actomyosin adjoining the lower leaflet of the bilayer applies stochastic contractile stresses on the membrane components that bind to it; these are the lower-leaflet PS ($\alpha = 3$) and the transmembrane protein TMABD ($\alpha = 6$), with binding affinities given by K_{PS} and K_{TM}, respectively.

Dynamics of segregation using kinetic Monte Carlo. The dynamics of the membrane components, subject to both equilibrium and active forces, are described in terms of a master equation for the time evolution of the probability distribution, $P(\{X_i^\alpha\}, \{\Omega_{\mathbf{x}_a}\}, t)$, where $\{X_i^\alpha\}$ is the set of positions of the ith particle of component α and $\{\Omega_{\mathbf{x}_a}\}$ are the placements of the active stress events centered at locations $\{\mathbf{x}_a\}$ with dimension ξ and lifetime τ. We solve the master equation using kinetic Monte Carlo updates that are determined both by equilibrium pair potentials and by the forces arising from the local contractile stress if the particles (PS and TMABD) are in the region $\{\Omega_{\mathbf{x}_a}\}$. The former is given by the usual metropolis transition probability and obeys detailed balance (68). The moves driven by the contractile stress break detailed balance and are applied based on the affinities, K_{PS} and K_{TM}, that allow PS or TMABD to preferentially move toward the center $\mathbf{x}_a$ through a series of biased exchange attempts.

Data Availability. All study data are included in the article and/or *SI Appendix*.

ACKNOWLEDGMENTS. We thank members of the laboratories of S.M. and M.R. for stimulating discussions and critical reading of the text and Andrey Klymchenko (University of Strasbourg) for the gift of Nile Red Dye (NR12S). S.S. acknowledges fellowship support from National Centre for Biological Sciences (NCBS)-Tata Institute for Fundamental Research (TIFR) and American Heart Association Grant 18POST33990156. A.D. acknowledges support from the Centre for Theoretical Biological Physics and the Discovery Cluster at Northeastern University. A.D. and M.R. acknowledge support from Simons Foundation Grant 287975. C.P. and P.S. acknowledge graduate fellowships from NCBS (TIFR). A.A.A. was supported by an National-Post Doctoral Fellowship from Department of Science and Technology, India. S.M. and M.R. are J. C. Bose Fellows (Department of Science and Technology, India), and S.M. acknowledges support from Human Frontier Science Program Grant RGP0027/2012 and Department of Biotechnology–Wellcome Trust India Alliance Margadarshi Fellowship IA/M/15/1/502018. MR and SM acknowledge support from the Department of Atomic Energy, India (under Project No. RTI 4006). We acknowledge support from the NCBS Central Imaging and Flow Facility computing facilities.

Author affiliations: [a]Cellular Organization and Signalling, National Centre for Biological Sciences, Tata Institute of Fundamental Research, Bangalore 560065, India; [b]Cardiovascular Research Institute, University of California, San Francisco, CA 94158; and [c]Department of Physics and Center for Theoretical Biological Physics, Northeastern University, Boston, MA 02115

1. M. Edidin, Lipids on the frontier: A century of cell-membrane bilayers. *Nat. Rev. Mol. Cell Biol.* **4**, 414–418 (2003).
2. D. Lingwood, K. Simons, Lipid rafts as a membrane-organizing principle. *Science* **327**, 46–50 (2010).
3. E. Sezgin, I. Levental, S. Mayor, C. Eggeling, The mystery of membrane organization: Composition, regulation and roles of lipid rafts. *Nat. Rev. Mol. Cell Biol.* **18**, 361–374 (2017).
4. S. J. Singer, G. L. Nicolson, The fluid mosaic model of the structure of cell membranes. *Science* **175**, 720–731 (1972).
5. K. Jacobson, E. D. Sheets, R. Simson, Revisiting the fluid mosaic model of membranes. *Science* **268**, 1441–1442 (1995).
6. K. Simons, E. Ikonen, Functional rafts in cell membranes. *Nature* **387**, 569–572 (1997).
7. D. Goswami *et al.*, Nanoclusters of GPI-anchored proteins are formed by cortical actin-driven activity. *Cell* **135**, 1085–1097 (2008).
8. K. Gowrishankar *et al.*, Active remodeling of cortical actin regulates spatiotemporal organization of cell surface molecules. *Cell* **149**, 1353–1367 (2012).
9. S. A. Freeman *et al.*, Transmembrane pickets connect cyto- and pericellular skeletons forming barriers to receptor engagement. *Cell* **172**, 305–317.e10 (2018).
10. P. Sil *et al.*, Dynamic actin-mediated nano-scale clustering of CD44 regulates its meso-scale organization at the plasma membrane. *Mol. Biol. Cell* **31**, 561–579 (2020).
11. R. Chandran, G. Kale, J. M. Philippe, T. Lecuit, S. Mayor, Distinct actin-dependent nanoscale assemblies underlie the dynamic and hierarchical organization of E-cadherin. *Curr. Biol.* **31**, 1726–1736.e4 (2021).
12. S. Arumugam *et al.*, Ceramide structure dictates glycosphingolipid nanodomain assembly and function. *Nat. Commun.* **12**, 3675 (2021).
13. M. F. Garcia-Parajo, A. Cambi, J. A. Torreno-Pina, N. Thompson, K. Jacobson, Nanoclustering as a dominant feature of plasma membrane organization. *J. Cell Sci.* **127**, 4995–5005 (2014).
14. K. Jacobson, P. Liu, B. C. Lagerholm, The lateral organization and mobility of plasma membrane components. *Cell* **177**, 806–819 (2019).
15. S. Saha, A. A. Anilkumar, S. Mayor, GPI-anchored protein organization and dynamics at the cell surface. *J. Lipid Res.* **57**, 159–175 (2016).
16. M. C. Marchetti *et al.*, Hydrodynamics of soft active matter. *Rev. Mod. Phys.* **85**, 1143 (2013).
17. M. Rao, S. Mayor, Active organization of membrane constituents in living cells. *Curr. Opin. Cell Biol.* **29**, 126–132 (2014).
18. A. Chaudhuri, B. Bhattacharya, K. Gowrishankar, S. Mayor, M. Rao, Spatiotemporal regulation of chemical reactions by active cytoskeletal remodeling. *Proc. Natl. Acad. Sci. U.S.A.* **108**, 14825–14830 (2011).
19. D. V. Köster *et al.*, Actomyosin dynamics drive local membrane component organization in an in vitro active composite layer. *Proc. Natl. Acad. Sci. U.S.A.* **113**, E1645–E1654 (2016).
20. K. Gowrishankar, M. Rao, Nonequilibrium phase transitions, fluctuations and correlations in an active contractile polar fluid. *Soft Matter* **12**, 2040–2046 (2016).
21. K. Husain, M. Rao, Emergent structures in an active polar fluid: Dynamics of shape, scattering, and merger. *Phys. Rev. Lett.* **118**, 078104 (2017).
22. S. R. Hossein, R. Mandal, M. Rao, Stratification, multivalency and turnover of the active cortical machinery are required for steady active contractile flows at the cell surface. arXiv [Preprint] (2021). https://arxiv.org/abs/2105.11358 (Accessed 21 May 2021).
23. S. Saha *et al.*, Diffusion of GPI-anchored proteins is influenced by the activity of dynamic cortical actin. *Mol. Biol. Cell* **26**, 4033–4045 (2015).
24. A. Das *et al.*, Stratification relieves constraints from steric hindrance in the generation of compact actomyosin asters at the membrane cortex. *Sci. Adv.* **6**, eaay6093 (2020).
25. P. Sharma *et al.*, Nanoscale organization of multiple GPI-anchored proteins in living cell membranes. *Cell* **116**, 577–589 (2004).
26. R. Varma, S. Mayor, GPI-anchored proteins are organized in submicron domains at the cell surface. *Nature* **394**, 798–801 (1998).
27. S. J. Plowman, C. Muncke, R. G. Parton, J. F. Hancock, H-ras, K-ras, and inner plasma membrane raft proteins operate in nanoclusters with differential dependence on the actin cytoskeleton. *Proc. Natl. Acad. Sci. U.S.A.* **102**, 15500–15505 (2005).
28. R. Raghupathy *et al.*, Transbilayer lipid interactions mediate nanoclustering of lipid-anchored proteins. *Cell* **161**, 581–594 (2015).
29. A. Das, A. Polley, M. Rao, Phase segregation of passive advective particles in an active medium. *Phys. Rev. Lett.* **116**, 068306 (2016).
30. A. Bansal, A. Das, M. Rao, Active segregation dynamics in the living cell. *Indian J. Phys.*, 10.1007/s12648–022–02298–z (2022).
31. S. Ghosh, S. Saha, D. Goswami, S. Bilgrami, S. Mayor, Dynamic imaging of homo-FRET in live cells by fluorescence anisotropy microscopy. *Methods Enzymol.* **505**, 291–327 (2012).
32. D. M. Owen, C. Rentero, A. Magenau, A. Abu-Siniyeh, K. Gaus, Quantitative imaging of membrane lipid order in cells and organisms. *Nat. Protoc.* **7**, 24–35 (2011).
33. P. Sengupta *et al.*, Probing protein heterogeneity in the plasma membrane using PALM and pair correlation analysis. *Nat. Methods* **8**, 969–975 (2011).
34. J. M. Kalappurakkal *et al.*, Integrin mechano-chemical signaling generates plasma membrane nanodomains that promote cell spreading. *Cell* **177**, 1738–1756.e23 (2019).
35. S. Saha, R. Raghupathy, S. Mayor, Homo-FRET imaging highlights the nanoscale organization of cell surface molecules. *Methods Mol. Biol.* **1251**, 151–173 (2015).
36. S. A. Rizvi *et al.*, Identification and characterization of a small molecule inhibitor of formin-mediated actin assembly. *Chem. Biol.* **16**, 1158–1168 (2009).
37. B. J. Nolen *et al.*, Characterization of two classes of small molecule inhibitors of Arp2/3 complex. *Nature* **460**, 1031–1034 (2009).
38. A. A. Anilkumar, PhD thesis, "Understanding the mechanism of coupling between the outer leaflet proteins and the actin cytoskeleton." SASTRA Deemed University, Tamilnadu, India (2016).
39. V. Mueller *et al.*, STED nanoscopy reveals molecular details of cholesterol- and cytoskeleton-modulated lipid interactions in living cells. *Biophys. J.* **101**, 1651–1660 (2011).
40. T. Baumgart *et al.*, Large-scale fluid/fluid phase separation of proteins and lipids in giant plasma membrane vesicles. *Proc. Natl. Acad. Sci. U.S.A.* **104**, 3165–3170 (2007).
41. T. Yeung *et al.*, Membrane phosphatidylserine regulates surface charge and protein localization. *Science* **319**, 210–213 (2008).
42. K. Gaus, S. Le Lay, N. Balasubramanian, M. A. Schwartz, Integrin-mediated adhesion regulates membrane order. *J. Cell Biol.* **174**, 725–734 (2006).
43. K. Gaus, T. Zech, T. Harder, Visualizing membrane microdomains by Laurdan 2-photon microscopy. *Mol. Membr. Biol.* **23**, 41–48 (2006).
44. D. M. Owen, D. J. Williamson, A. Magenau, K. Gaus, Sub-resolution lipid domains exist in the plasma membrane and regulate protein diffusion and distribution. *Nat. Commun.* **3**, 1256 (2012).
45. M. S. Jaureguiberry *et al.*, Membrane organization and regulation of cellular cholesterol homeostasis. *J. Membr. Biol.* **234**, 183–194 (2010).
46. H. J. Kaiser *et al.*, Order of lipid phases in model and plasma membranes. *Proc. Natl. Acad. Sci. U.S.A.* **106**, 16645–16650 (2009).
47. D. B. Iaea, F. R. Maxfield, Membrane order in the plasma membrane and endocytic recycling compartment. *PLoS One* **12**, e0188041 (2017).
48. O. A. Kucherak *et al.*, Switchable nile red-based probe for cholesterol and lipid order at the outer leaflet of biomembranes. *J. Am. Chem. Soc.* **132**, 4907–4916 (2010).
49. J. M. Kalappurakkal, P. Sil, S. Mayor, Toward a new picture of the living plasma membrane. *Protein Sci.* **29**, 1355–1365 (2020).
50. G. J. Doherty, H. T. McMahon, Mediation, modulation, and consequences of membrane-cytoskeleton interactions. *Annu. Rev. Biophys.* **37**, 65–95 (2008).
51. T. Lecuit, A. S. Yap, E-cadherin junctions as active mechanical integrators in tissue dynamics. *Nat. Cell Biol.* **17**, 533–539 (2015).
52. T. S. van Zanten *et al.*, Hotspots of GPI-anchored proteins and integrin nanoclusters function as nucleation sites for cell adhesion. *Proc. Natl. Acad. Sci. U.S.A.* **106**, 18557–18562 (2009).
53. C. Bernardini, S. D. Stoyanov, L. N. Arnaudov, M. A. Cohen Stuart, Colloids in Flatland: A perspective on 2D phase-separated systems, characterisation methods, and lineactant design. *Chem. Soc. Rev.* **42**, 2100–2129 (2013).
54. R. Brewster, S. A. Safran, Line active hybrid lipids determine domain size in phase separation of saturated and unsaturated lipids. *Biophys. J.* **98**, L21–L23 (2010).
55. M. Schick, Membrane heterogeneity: Manifestation of a curvature-induced microemulsion. *Phys. Rev. E Stat. Nonlin. Soft Matter Phys.* **85**, 031902 (2012).
56. M. Schick, Strongly correlated rafts in both leaves of an asymmetric bilayer. *J. Phys. Chem. B* **122**, 3251–3258 (2018).
57. B. A. Truong Quang, M. Mani, O. Markova, T. Lecuit, P. F. Lenne, Principles of E-cadherin supramolecular organization in vivo. *Curr. Biol.* **23**, 2197–2207 (2013).
58. Y. Shin, C. P. Brangwynne, Liquid phase condensation in cell physiology and disease. *Science* **357**, eaaf4382 (2017).
59. D. Bracha, M. T. Walls, C. P. Brangwynne, Probing and engineering liquid-phase organelles. *Nat. Biotechnol.* **37**, 1435–1445 (2019).
60. S. F. Banani, H. O. Lee, A. A. Hyman, M. K. Rosen, Biomolecular condensates: Organizers of cellular biochemistry. *Nat. Rev. Mol. Cell Biol.* **18**, 285–298 (2017).
61. C. A. Weber, D. Zwicker, F. Jülicher, C. F. Lee, Physics of active emulsions. *Rep. Prog. Phys.* **82**, 064601 (2019).
62. N. Zanin, C. Viaris de Lesegno, C. Lamaze, C. M. Blouin, Interferon receptor trafficking and signaling: Journey to the cross roads. *Front. Immunol.* **11**, 615603 (2021).
63. S. Saha, T. L. Nagy, O. D. Weiner, Joining forces: Crosstalk between biochemical signalling and physical forces orchestrates cellular polarity and dynamics. *Philos. Trans. R. Soc. B Biol. Sci.* **373**, 20170145 (2018).
64. M. Wu, J. Liu, Mechanobiology in cortical waves and oscillations. *Curr. Opin. Cell Biol.* **68**, 45–54 (2021).
65. A. W. C. Lau, B. D. Hoffman, A. Davies, J. C. Crocker, T. C. Lubensky, Microrheology, stress fluctuations, and active behavior of living cells. *Phys. Rev. Lett.* **91**, 198101 (2003).
66. A. Basu, J. F. Joanny, F. Jülicher, J. Prost, Thermal and non-thermal fluctuations in active polar gels. *Eur Phys J E Soft Matter* **27**, 149–160 (2008).
67. A. Singh Vishen, J. F. Rupprecht, G. V. Shivashankar, J. Prost, M. Rao, Soft inclusion in a confined fluctuating active gel. *Phys. Rev. E* **97**, 032602 (2018).
68. D. P. Landau, K. Binder, *A Guide to Monte Carlo Simulations in Statistical Physics* (Cambridge University Press, 2005).